Lithography of high spatial density biosensor structures with sub-100 nm spacing by MeV proton beam writing with minimal proximity effect

Harry J Whitlow[1,2,3,6]**, May Ling Ng**[1,2,7]**, Vaida Auželyté**[1,2]**,
Ivan Maximov**[2,4]**, Lars Montelius**[2,4]**, Jeroen A van Kan**[5]**,
Andrew A Bettiol**[5] **and Frank Watt**[5]

[1] Division of Nuclear Physics, Lund Institute of Technology, PO Box 118,
SE-221 00 Lund, Sweden
[2] The Nanometre Consortium, Box 118, SE-221 000 Lund, Sweden
[3] School of Technology and Society, Malmö högskola, SE-205 06 Malmö, Sweden
[4] Division of Solid State Physics, Lund Institute of Technology, PO Box 118,
SE-221 00 Lund, Sweden
[5] Centre for Ion Beam Applications, Department of Physics, National University of
Singapore, 2 Science Drive 3, Singapore 117542, Singapore

E-mail: Harry_J.Whitlow@nuclear.lu.se

Abstract
Metal electrode structures for biosensors with a high spatial density and
∼85 nm gaps have been produced using focused megaelectronvolt (MeV)
proton beam writing of poly-(methyl methacrylate) positive resist combined
with metal lift-off. The minimal proximity exposure and straight proton
trajectories in (∼100 nm) resist layers for focused MeV proton beam writing
are strongly indicative that ultimate electrode gap widths approaching a few
nanometres are achievable.

1. Introduction

Assaying biomolecules by measurement of the electrical impedance between interdigitated electrodes in an electrochemical cell is of great topical interest. The change in electrical admittance between interdigitated electrodes with e.g. specific receptor molecules immobilized on the surface is determined by the presence of the specific target molecule [1, 2]. These sensors are applicable for an extremely broad range of immunoassay applications from detecting simple toxins such as formaldehyde [3] to measuring bacterial metabolism [4] and detection of specific large molecules such as specific DNA sequences and hormones [1, 5]. In more sophisticated indirect measurements the detection of HIV antibodies has been reported [6]. Much current interest is focused

on sensors based on nanoscale electrode arrays with a high electrode spatial density and electrode gap d of 10–300 nm because:

- The sensitivity is enhanced for $d \sim$ 10–200 nm compared to conventional sensors with d on a scale of 0.5–1000 μm because of the geometric effect associated with the high electrode spatial density [7, 8] and also because the current flow in the cell is confined to a thin surface layer with thickness of the order of the electrode gap, within which the receptor molecules are immobilized [9].
- The electric field for a modest 100 mV voltages with $d = 100$ nm yields 1 MV m^{-1} electric fields that may induce non-linear dipole effects that can be exploited to enhance specificity and sensitivity as well as shifting relaxation phenomena to an accessible region of the frequency spectrum [7].
- Only a small potential difference is needed to operate the cell, which minimizes the influence of disturbance

---

[6] Author to whom any correspondence should be addressed.
[7] Present address: Singapore Synchrotron Light Source, National University of Singapore, 5 Research Link, Singapore 117603, Singapore.

from electrochemical reactions with the electrode materials [7, 8].

- The increase in sensitivity and geometrical size implies that smaller quantities of analyte are needed which is an important consideration for lab-on-a-chip applications using e.g. multi-sensor [8] and DNA sequence sensor [5] arrays.

Nanoscale interdigitated electrode structures are also of great importance for high electron mobility transistors (HEMT), strip readout Si detectors [10] and also organic FETs [11]. The fabrication of these structures is technically challenging. This is because the combined requirements of small electrode gaps (large fields), wide metal electrodes (minimum parasitic series resistance) and large number of electrodes (large sensitivity) requires writing high spatial density metal patterns with a metal-width to gap width ratio considerably greater than one.

The metal lift-off process is well suited for fabricating interdigitated biosensor structures. Metal lift-off with conventional electron beam lithography (EBL) is non-trivial for nanometre structures with high spatial density because of the need to accurately characterize and correct for the effect of proximity exposure [12]. The proximity exposure effect is particularly troublesome for high spatial density patterns especially where the exposed area significantly exceeds the unexposed area. The writing of nanoscale structures in thin resist materials with low energy and heavy ion beams has been demonstrated with a focused ion beam (FIB) [13, 14]. The use of patterns written in resist for metal lift-off is preferable to direct writing methods (e.g. using a FIB to decompose gaseous precursors [15]) because of the absence of 'overspray' in the gaps. However, as far as we are aware, low-energy FIB has not been used for pattern writing in combination with metal lift-off on a nanoscale. Generally, successful metal lift-off requires vertical, or slightly undercut, edges in the resist pattern after development. Although successful lift-off has been accomplished with a 1:1 metal to resist thickness ratio using a sophisticated multilayer resist/multi-developer process in combination with dry etching [16, 17], a 1:~3 metal to resist ratio allows straightforward processing with a single developer. The combination of small gaps, vertical edges and thick resist implies that the pattern in resist after development must be written with a high vertical to horizontal aspect ratio. Low-energy FIB is poorly suited to writing such high aspect ratio structures in poly-(methyl methacrylate) (PMMA) because of the short range (e.g. ~50 nm for 30 keV ^{69}Ga$^+$) and the strong nuclear scattering induced lateral spreading imply only thin (e.g. 50 nm) films can be written. Recently the use of proton beam writing (p-beam writing) with focused MeV proton beams to write extreme vertical to horizontal aspect ratio (~100:1) sub-100 nm structures in resist has been demonstrated [18]. Here the high aspect ratio and spatial density writing capabilities of p-beam writing have been explored for metal lift-off fabrication of interdigitated nanoscale biosensors test structures.

2. Comparison of proximity exposure for proton and electron beam writing

The feature dimensions that can be written by a focused particle beam in resist material is determined by the extent of the region

where the introduced dose exceeds the threshold required to induce a developable latent effect. The two-dimensional dose distribution about a single point $G(\mathbf{r})$ is then represented by a convolution of the beam focus profile, $F(\mathbf{r})$, with the dose distribution, $D(\mathbf{r}')$, which arises from spatial spreading of the beam in the target material and those secondary particles that contribute to the dose. $G(\mathbf{r}) = \int_{\text{all } \mathbf{r}'} d\mathbf{r}' \cdot F(\mathbf{r}) \cdot D(\mathbf{r} - \mathbf{r}')$, with $\mathbf{r}$ and $\mathbf{r}'$ being position vectors from the axes of the beam and ion impingement axis, respectively. Generally, for pattern writing both the width and shape of the $G(\mathbf{r})$ distribution are important. It is convenient to consider the contributions $D(\mathbf{r})$, $F(\mathbf{r})$ separately. $D(\mathbf{r})$ represents an *intrinsic* limiting contribution to $G(\mathbf{r})$ that is governed by the physics of the interaction between the particle and target material and, trivially, $G(\mathbf{r}) = D(\mathbf{r})$ for a perfectly focused beam. $F(\mathbf{r})$ on the other hand represents an *extrinsic* contribution that can (at least in principle) be improved by technical enhancement of focusing and mechanical and electronic stability. In practice the dose distribution $G(\mathbf{r})$ is finite even at quite large $\mathbf{r}$ which has the important consequence that energy is deposited in regions of the pattern that are unirradiated but are in close proximity to irradiated regions. This is due to the spreading of the dose over edges of irradiated regions. This is termed the *proximity exposure* and is particularly troublesome for patterns with small features and large spatial density such as interdigitated electrode arrays.

The intrinsic exposure contribution from particle–matter interactions, $D(\mathbf{r})$, presents an ultimate limit to the achievable spatial density, feature size and aspect ratio. The effect of the proximity exposure in EBL can be judged from figure 1, which compares the calculated dose distributions for 39 keV electrons and 1 MeV H$^+$ ions [19] across the edge of a semi-infinite irradiated area with a straight boundary [20] in PMMA. The electron dose was obtained by numerical integration of the empirical radial dose distribution function [13]:

$$D(r) = \frac{1}{\pi(\eta+1)}\left[\frac{1}{\alpha^2}\exp\left(-\frac{r^2}{\alpha^2}\right) + \frac{\eta}{\beta^2}\exp\left(-\frac{r^2}{\beta^2}\right)\right], \quad (1)$$

where, α, β and η were taken to be 50.1, 5380 nm and 0.7, respectively, which corresponds to the fitted values for 100 nm PMMA on Si for the Lund JSM 6400 EBL system with a RAITH pattern generator and control software. The instrumental focus contribution to the fitted values was not corrected for because the beam spot radius (1–3 nm) is much smaller than α and β which represent the widths at $1/e$ amplitude of the forward-scattered and backscattered contributions to $D(r)$ respectively. The remaining parameter, η, which is the integral ratio of the backscattered to primary intensities will only be weakly influenced by the focus.

To determine the corresponding radial dose dependence $D(r)$ for 1 MeV protons the secondary electron range R (nm) $= 0.012E(\text{eV})^{1.274}$ in PMMA was determined by fitting literature data [21–23]. Using this empirical relation the dose from the edge from a straight boundary to a semi-infinite irradiated area (figure 1, inset) was subsequently calculated [24] with Waligórski *et al*'s [25] correction for protons. The sharper dose fall-off outside the irradiated region seen in figure 1 for protons with $d < 30$ nm coupled with the small calculated [26] lateral spread of primary ion trajectories in the outer 100 nm of resist
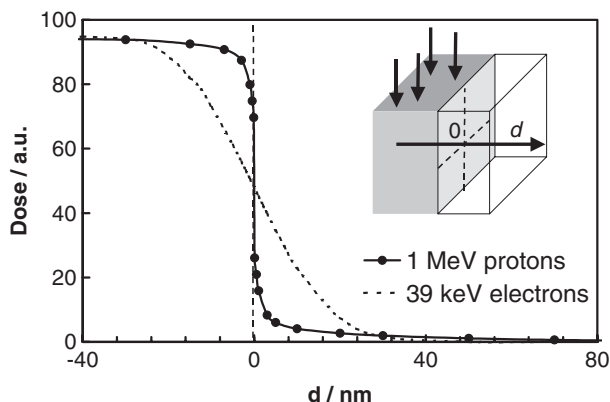
Figure 1. Intrinsic contributions to the dose distributions calculated following [22] for 39 keV electrons and 1 MeV protons with the correction of Waligórski *et al* [24, 25]. The curves are normalized at $d = -30$ nm.

(∼0.2 nm half width tenth maximum (HWTM)) implies that the proximity exposure effect is considerably smaller for p-beam writing in the edge region than for EBL. For 1 MeV $^1H^+$ the dose contribution from backscattering processes is negligible because of the vanishingly small cross section for ion backscattering from the substrate and the short range (<10 nm) of the quasi-elastic secondary electrons. Proton induced x-ray kerma associated effects will make only a small contribution to $D(r)$ and were neglected. The aspect ratio is then primarily governed by the lateral spread of the primary ion trajectories [24]. For the low-energy FIB case the corresponding calculated radial broadening after traversing 100 nm of PMMA is 3 and 30 nm HWTM for 30 keV protons or 100 keV $^{69}Ga^+$ ions, respectively, which is much larger than the corresponding value of 0.2 nm HWTM for 1 MeV H^+ p-beam writing.

The extrinsic contribution to the spreading of the dose distribution is governed by the beam focus and other disturbing factors such as mechanical and electrical instability. In EBL, field emission sources combined with cylindrical lenses allow focusing of lithographic beams with a focus better than a few nanometres. The proximity exposure is then governed by the spatial spread of the electron dose distribution as discussed above.

For p-beam writing the broadening of the dose distribution from both the spatial extent of the energy deposited by electrons and the spreading from nuclear scattering is considerably smaller than the extrinsic contribution from the beam focus, which is currently on a scale of tens of nanometres. It follows that p-beam writing is a useful complement to both conventional EBL and low-energy FIB writing. This is because the smaller proximity exposure and nuclear scattering-induced lateral spread for p-beam writing opens up the possibility of writing nanometre structures with high spatial density and large height/width aspect ratios. This is borne out by recent demonstrations [19, 20, 27] of lithography with 8–100 aspect ratios at micrometre dimensions by megaelectronvolt p-beam writing.

3. Experimental details

A 300 nm thick SiO_2 layer was grown on (100)Si by wet oxidation. Two layers of PMMA positive resist with
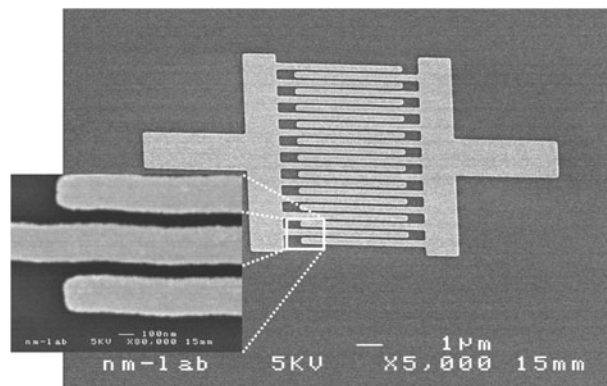
molecular weight 20 000 and 950 000 u and thickness ∼85 and ∼70 nm, respectively, were subsequently deposited by spinning. Exposure was carried out using the new p-beam writing facility at the National University of Singapore using 2 MeV H_2^+ ions. The beam size was measured [28] using a Ni calibration grid to be 100 nm FWHM (full width half maximum) in the horizontal and vertical directions. The beam current was ∼7 fA and the spot was vector rastered over the pattern six times with constant speed with a dwell time of 273 μs per 10 nm × 10 nm pixel step. A pixel writing fluence 50% greater than the clearing fluence of 5×10^{13} H_2^+ ions cm^{-2} (80 nC mm^{-2}) was used to correct for the finite beam size. A set of similar patterns was written with identical exposed line widths (200 nm) and unexposed gap widths from 140, 280 and 220 nm. No correction for proximity exposure was applied. Resist development was for 30 s in a mixture by volume of 60% diethylene glycol, monobytyl ether 20%, morpholine 5% ethanolamine, balance H_2O, followed by a 30 s rinse in water. Blanket metal layers of 3 nm of Ti followed by 25 nm Au were deposited by e-beam evaporation and metal lift-off was carried out in hot acetone.

4. Results

Figure 2 shows a SEM image of a prototype biosensor structure. The interdigitated electrode pattern written consisted of 210 nm wide bars with a gap of 130 nm. The internal corners in the metal pattern after lift-off have a radius of ∼55 nm which is consistent with a resolution limited by beam spot extent. The width of the metal contacts and the waviness of the edges of the lines were determined from ∼60 ocular measurements against a millimetre scale for each sample on high magnification micrographs. The mean gap for the structure in figure 2 is 84 nm. For all the samples the mean spreading of 22 nm outside of the exposed region and the standard deviation (error bars in figure 3) from a straight edge (edge waviness) shows no evidence of dependence on the width of the gap in the written pattern (figure 3). The 22 nm mean spreading is much smaller than the width of the edge (<5 nm) seen in the results of the theoretical estimation (figure 1). (The 2 MeV H_2^+ molecular ions fragment on penetrating the surface into two 1 MeV protons.) This implies that the edge spreading is not limited by the proximity exposure from proton–matter

Figure 2. SEM image of the prototype nano-biosensor structure after metal lift-off.
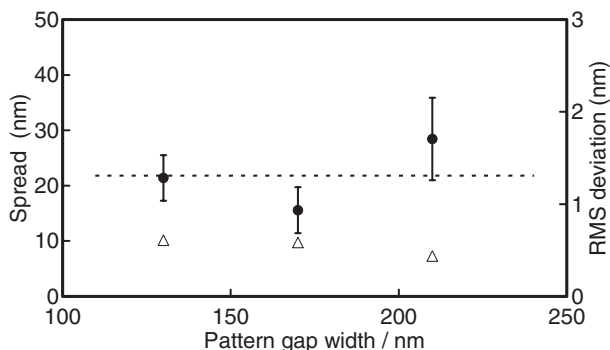
Figure 3. Spreading of the edge of the metal bar beyond the pattern edge (circles, left vertical scale). The horizontal dotted line represents the mean value of the spreading. The triangles denote the standard deviation from a straight line extending along the edge (right vertical scale).

interactions, but instead determined by the size ($\sim$100 nm) of the beam spot used here. From the sharpness of the calculated dose fall-off across an edge for proton beam writing (figure 1), it follows that straightforward technical improvements such as improved focusing procedures, mechanical stability and reduction of electrical noise can reduce the attainable gap width towards the ultimate (figure 1) of a few nanometres. Very recent work has shown that protons can be focused down to 35 nm FWHM [28] and writing a line $\sim$30 nm wide between exposed regions in 70 nm thick 950 000 u PMMA has been demonstrated [29].

5. Summary

Prototype biosensor structures with gaps between metal electrode fingers of $\sim$85 nm have been successfully written using focused MeV p-beam writing. The ($\sim$22 nm) spreading of the metal after lift-off outside the irradiated area chiefly due to the beam spot size which can be reduced further. This suggests that the technique has great potential by complementing conventional EBL for cases where the restrictions imposed by proximity exposure and limited aspect ratio are troublesome.

Acknowledgments

References

[1] Bergren C, Bjarneson B and Johansson G 2001 *Electroanalysis* **13** 173
[2] Gallado Soto A M, Jaffari S A and Bone S 2001 *Biosensors Bioelectron.* **16** 23
[3] Dzyadevch S, Arkhypova A A, Korpan Y I, El'skaya A V, Soldatkin A P, Jaffrezic-Renault N and Martelet C 2001 *Anal. Chim. Acta* **445** 47
[4] Gómez R, Bashir R and Bhunia A K 2002 *Sensors Actuators* B **86** 198
[5] Thews R, Hofmann F, Frey A, Holzpfl B, Scienle M, Paulus C, Schindler P, Ekstein G, Kassel C, Stanzel M, Hintsche R, Nebling E, Albers J, Hassman J, Schülein J, Goemann W and Gumbrecht W 2002 *Proc. ISSCC 2002* (San Francisco: IEEE) p 470
[6] Bresler H S, Lenkevich M J, Murdock J F, Newman A L and Roblin R O 1992 *ACS Symp. Series* vol 511 (Washington DC: American Chemical Society) p 89
[7] Montelius L, Tegenfeldt J O and Ling T G I 1995 *J. Vac. Sci. Technol.* A **13** 1755
[8] Montelius L, Heidari B, Graczyk M, Maximov I, Sarwe E-L and Ling T G I 2002 *Microelectron. Eng.* **53** 521
[9] van Gerwin P, Laureys W, Huyberechts G, Op De Beeck M, Baert K, Suls J, Varlan A, Sansen W, Hermans L and Mertens R 1997 *Transducers 97 (Chicago, 1997)* (Chicago: IEEE) p 907
[10] Rosolen G C 1999 *Appl. Surf. Sci.* **144/145** 467
[11] Clavio Cedñeo C, Seekamp J, Kam A P, Hoffmann T, Zankoych S, Sotomayer Tores C M, Menozzi C, Cavallini M, Mugia M, Ruani G, Biscarini F, Behl M, Zentel R and Ahopelto J 2002 *Microelectron. Eng.* **61/62** 25
[12] Aristov V V, Gaifullin B N, Svintsov A A, Zaitsev S I, Raith H F and Jede R 1992 *J. Vac. Sci. Technol.* B **10** 2459
[13] Matsuir S, Kojima Y and Ochiai Y 1988 *Appl. Phys. Lett.* **53** 868
[14] Gierak J, Vieu C, Schneider M, Launois H, Assayag G B and Septier A 1997 *J. Vac. Sci. Technol.* B **15** 2373
[15] Ling T, Stivers A, Livengood R, Yan P-Y, Zhang G and Lo F-C 2000 *J. Vac. Sci. Technol.* B **18** 3216
[16] Grundbacher R, Youtsey C and Adesida I 1996 *Microelectron. Eng.* **30** 317
[17] Grundbacher R, Adesida I, Kao Y-C and Ketterson A A 1997 *J. Vac. Sci. Technol.* B **15** 49
[18] van Kan J A, Bettiol A A and Watt F 2003 *Appl. Phys. Lett.* **83** 1629
[19] van Kan J A, Sum T C, Osipowicz T and Watt F 2000 *Nucl. Instrum. Methods* B **161–163** 366
[20] Osipowicz T, van Kan J A, Sum T C, Sanchez J L and Watt F 2000 *Nucl. Instrum. Methods* B **161–163** 83
[21] Raishton S A 1983 *Proc. 10th Int. Conf. on Electron and Ion Beam Science and Technology* ed R Bakish (Princeton, NJ: Electrochemical Society)
[22] Peterson P A, Radzimski Z J, Schwalm S A and Russel P E 1992 *J. Vac. Sci. Technol.* B **10** 3088
[23] McCord M A and Newham T H 1992 *J. Vac. Sci. Technol.* B **10** 3083
[24] Springham S V, Osipowicz T, Sanchez J L, Gan L H and Watt F 1997 *Nucl. Instrum. Methods* B **130** 155
[25] Walligórski M P R, Hann R N and Katz R 1986 *Nucl. Tracks Radiat. Meas.* **11** 309
[26] Ziegler J F 2000 *SRIM version 2000.20* available from http://www.srim.org
[27] van Kan J A, Sanchez J L, Osipowicz T and Watt F 2000 *Microsyst. Technol.* **6** 82
[28] Watt F, van Kan J A, Ratja I, Bettiol A A, Choo T F, Breese M B H and Osipowicz T 2003 *Nucl. Instrum. Methods* B **210** 14
[29] van Kan J A, Betiol A A and Watt F 2003 *Appl. Phys. Lett.* **83** 1629